Available online at www.sciencedirect.com
SCIENCE DIRECT®
Journal of Power Sources 119–121 (2003) 290–294
JOURNAL OF POWER SOURCES
www.elsevier.com/locate/jpowsour

Low-crystalline β-FeOOH and vanadium ferrite for positive active materials of lithium secondary cells

Atsushi Funabiki*, Hideo Yasuda, Masanori Yamachi

Fundamental Technology Laboratory, Corporate R&D Center, Japan Storage Battery Co. Ltd., Nishinosho, Kisshoin, Minami-ku, Kyoto 601-8520, Japan

Abstract

Low-crystalline β-FeOOH and vanadium ferrite were prepared by a simple hydrolysis method. XRD measurement revealed that the former material had a framework of β-FeOOH with somewhat amorphous structure, and that the latter one gave a crystalline structure analogous to that of the hydrated iron orthovanadate. From the electrochemical measurements, it was found that the low-crystalline β-FeOOH positive electrode showed a discharge capacity of 230 mAh/g in the potential range of 4.3 V and 1.6 V versus Li/Li^+, and better cycle performance than the high-crystalline one. The vanadium ferrite positive electrode also showed a high discharge capacity over 300 mAh/g and superior cycle performance.

Keywords: β-FeOOH; PVdF; Vanadium ferrite positive electrode

1. Introduction

A growing demand of high-energy-density power sources have created lithium secondary cells that employ lithium-transition-metal oxides and carbon as positive and negative active materials, respectively. For the lithium-transition-metal oxides, $LiCoO_2$, $LiNiO_2$, and $LiMn_2O_4$ have been used to provide 4V-class cells. These active materials, however, are rather costly, thus stimulating the development of more inexpensive positive active materials containing iron, because iron is much more abundant and inexpensive than cobalt, nickel, and manganese.

A number of iron-based materials have been investigated for use as positive active materials of lithium secondary cells; e.g. $LiFeO_2$ [1–3], $LiFePO_4$ [4,5], γ-FeOOH derivatives [6], $Fe_4[Fe(CH)_6]$ [7], and β-FeOOH [8]. Among them, the iron-based materials on Fe^{2+}/Fe^{3+} redox couple reaction have attracted much more attention because of its better reversibility.

Amine et al. focused on the β-type material with (2 × 2) tunnel structure [8] among several kinds of FeOOH. They found that the β-FeOOH positive electrode exhibited a high discharge capacity of over 200 mAh/g. However, this high-crystalline material had a drawback of poor cycle performance. In this work, the β-FeOOH has been further intensively studied on the relationship between its crystalline structure and electrochemical properties, and it has been found that the low-crystalline β-FeOOH positive electrode showed better cycle performance. Furthermore, in the course of preparing the low-crystalline material, a new iron-based vanadium oxide (vanadium ferrite) delivering the high discharge capacity over 300 mAh/g has been obtained. This paper reports the structure, composition, and electrochemical properties of low-crystalline β-FeOOH and vanadium ferrite positive active materials.

2. Experimental

2.1. Synthesis of active materials

The low-crystalline β-FeOOH was prepared by simply hydrolyzing a mixture of $FeCl_3 \cdot 6H_2O$ and sulfates such as $CuSO_4 \cdot 5H_2O$, $Al_2(SO_4)_3 \cdot 8H_2O$, $Li_2SO_4 \cdot H_2O$, and $VOSO_4 \cdot 2H_2O$. On the other hand, the replacement of the sulfate with other salts such as chloride and nitrate produced a high-crystalline phase. These facts suggest that the nature of the solution for the hydrolysis has a great effect on the crystallinity of β-FeOOH. When $VOSO_4$ was used as the sulfate, the structure of the product was dependent on the concentration of the salt; the low-crystalline β-FeOOH was formed

* Corresponding author. Tel.: +81-75-316-3611; fax: +81-75-312-1261.
E-mail address: atsushi_funabiki@gs.nippondenchi.co.jp (A. Funabiki).

0378-7753/03/$ – see front matter © 2003 Elsevier Science B.V. All rights reserved.
doi:10.1016/S0378-7753(03)00156-3

Table 1
The amount of salts dissolved in the solution of 300 ml for the hydrolysis

Active material	$FeCl_3 \cdot 6H_2O$ (mol)	$CuSO_4 \cdot 5H_2O$ (mol)	$VOSO_4 \cdot 2H_2O$ (mol)
High-crystalline β-FeOOH	0.090	0	0
Low-crystalline β-FeOOH	0.030	0.030	0
Vanadium ferrite	0.030	0	0.0035

when the molar ratio of $VOSO_4/FeCl_3$ was less than 0.1, while a higher molar ratio resulted in vanadium ferrite. A high-crystalline material was also prepared by hydrolyzing $FeCl_3 \cdot 6H_2O$ for comparison. Table 1 summarizes the amount of salts dissolved in the solution for the hydrolysis to prepare each active material. The resulting aqueous solutions were slowly hydrolyzed at 60–80 °C, and subsequently aged for 1 day. During the reaction, a precipitation took place. After the filtration of the precipitate, it was washed with deionized water and then dried in air at 60 °C.

2.2. Electrochemical measurements

Electrochemical measurements were carried out in three-electrode flooded-type cells. The working electrode was prepared by mixing the obtained active materials (75 wt.%), acetylene black (20 wt.%), and poly(vinylidene fluoride) (PVdF) (5 wt.%) with *N*-methyl-2-pyrrolidone (NMP), and spreading the resulting slurry on an aluminum mesh. The electrode was pressed at 1 t/cm^2, and then dried in vacuum at 100 °C for 12 h. The size of the electrode was 1.5 cm × 1.5 cm × 0.04 cm. Metallic lithium was used for counter and reference electrodes. The electrolytic solution was 1 M $LiClO_4$ dissolved in a 2:2:1 (by volume) mixture of ethylene carbonate (EC), dimethyl carbonate (DMC), and diethyl carbonate (DEC). The test cells were discharged and charged between the cut-off potentials of 1.6 V and 4.3 V (versus Li/Li$^+$) at a constant current of 0.1*C* mA, where C is the numerical value of the theoretical discharge capacity of β-FeOOH (302 mAh/g). All measurements were conducted at room temperature (25 °C) in an argon-filled glove box.

3. Results and discussion

3.1. Structure and composition of the active materials

The crystalline structure and composition of the obtained active materials were investigated by X-ray diffractometry (XRD) and elemental analysis. Fig. 1(a)–(c) show XRD patterns of the high-, and low-crystalline β-FeOOH, and vanadium ferrite, respectively. The low-crystalline β-FeOOH exhibited more broad peaks than the high-crystalline one, indicating that the former material had a framework of β-FeOOH with a somewhat amorphous structure. The vanadium ferrite in Fig. 1(c) gave a pattern greatly different

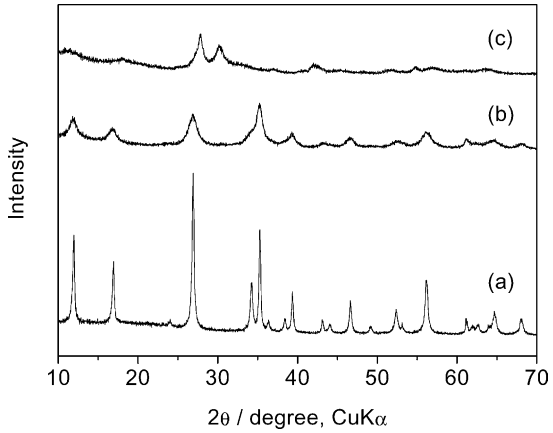

Fig. 1. XRD patterns of the (a) high-crystalline β-FeOOH, (b) low-crystalline β-FeOOH, and (c) vanadium ferrite.

Table 2
Elemental analysis results of the active materials

Active material	Fe (wt.%)	Cl (wt.%)	S (wt.%)	V (wt.%)
High-crystalline β-FeOOH	55	4	–[a]	–
Low-crystalline β-FeOOH	54	2	3	–
Vanadium ferrite	35	–	0.5	25

[a] The amount of element less than 0.1 wt.% is represented by –.

from those of the β-FeOOH in Fig. 1(a) and (b); two definite peaks appear at around 28° and 30°. This feature is very similar to that of the recently reported hydrated iron orthovanadate ($FeVO_4 \cdot 1.1H_2O$) [9].

The weight ratio of elements in each active material determined by elemental analysis is listed in Table 2. Compared with the high-crystalline β-FeOOH, the low-crystalline one contained a larger amount of sulfur which originates from metal sulfate dissolved in the solution subjected to the hydrolysis. This result suggests that the incorporation of sulfur into β-FeOOH may have inhibited the progress of its crystallinity.

It is well known that β-FeOOH contains water molecules within the (2 × 2) tunnel [10] in addition to the incorporated elements like chlorine listed in Table 2. The approximate amount of water contained in the samples was calculated from the results in Table 1. The formulas of the high-, and low-crystalline β-FeOOH thus determined are expressed as $FeOOHCl_{0.1} \cdot 0.4H_2O$ and $FeOOHCl_{0.06}S_{0.1} \cdot 0.5H_2O$, respectively.

The vanadium ferrite and the reported iron orthovanadate gave analogous crystalline structures as noted above. Each material, however, differed in its composition; the atomic ratio of Fe/V was 1.2 for the former and 1.0 for the latter. These results suggest that the vanadium ferrite obtained in this work is to be regarded as a new iron-based vanadium oxide.

3.2. Particle morphology and diameter of the β-FeOOH

The observation by scanning electron microscopy (SEM) revealed that the particle morphology was needle-like for the high-crystalline β-FeOOH, while aggregated for the low-crystalline one. From the measurement of the particle size distribution, the average particle diameters of the high-, and low-crystalline one were found to be 0.5 mm and 5.0 μm, respectively.

3.3. Electrochemical properties of the β-FeOOH and vanadium ferrite positive electrodes

3.3.1. β-FeOOH positive electrode

Fig. 2 shows the discharge and charge characteristics of the high-, and low-crystalline β-FeOOH positive electrodes in the first cycle. Both electrodes exhibited an initial discharge capacity of around 230 mAh/g. The electrochemical reaction mechanism for β-FeOOH is expressed as the following Fe^{2+}/Fe^{3+} redox couple:

$$FeOOH + Li^+ + e^- \leftrightarrows LiFeOOH \quad (1)$$

The theoretical discharge capacity of β-FeOOH based on reaction (1) is 302 mAh/g. The discharge capacity of 230 mAh/g in this work indicates that the utilization of the prepared active material was 75%. The main reason for this low utilization is attributable to the substantial amount of the impurities such as H_2O, Cl, and S which occupy around 10 wt.% or more of the total mass of the active materials.

A close look at the discharge and charge curves of the high-, and low-crystalline β-FeOOH positive electrodes in Fig. 2 revealed that the former electrode showed an abrupt drop in potential in the initial stage in the first discharge, followed by a potential plateau at around 2.0 V that covered most of the capacity, whereas the latter electrode exhibited a gradual change in potential. On the other hand, each electrode had a similar shape of the curves during the first charge and the following cycles, suggesting that the high-, and low-crystalline β-FeOOH was changed to a similar structure during the first discharging process.

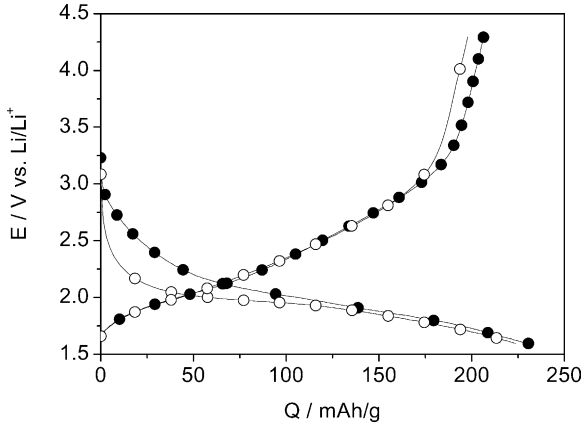

Fig. 2. Discharge and charge characteristics of the (○) high-crystalline β-FeOOH, (●) low-crystalline β-FeOOH positive electrodes in the first cycle.

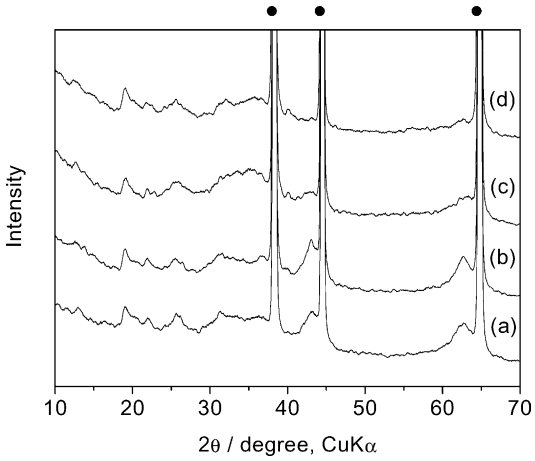

Fig. 3. XRD patterns of the (a, c) high-crystalline β-FeOOH positive electrodes, and (b, d) low-crystalline β-FeOOH positive electrodes. The electrodes were discharged to (a, b) 1.6 V, and charged to (c, d) 4.3 V in the first cycle. A symbol (●) denotes the diffraction peak due to aluminum. Small peaks at around 19 and 26° are due to PVdF and acetylene black, respectively.

The structural change of these two samples after the initial discharge and charge was investigated by XRD measurement. Fig. 3(a) and (b) show XRD patterns of the discharged high-, and low-crystalline β-FeOOH electrodes, respectively, and Fig. 3(c) and (d) present those of the charged electrodes. The two electrodes exhibited similar diffraction patterns with new peaks at around 43° and 63° when discharged to 1.6 V, and the intensity of these peaks drastically decreased when charged to 4.3 V, resulting in a very broad pattern. This fact indicates that the crystalline structure of β-FeOOH changed during the first discharge and became amorphous after one cycle.

Fig. 4 shows the cycle performance of the high-, and low-crystalline β-FeOOH positive electrodes, respectively.

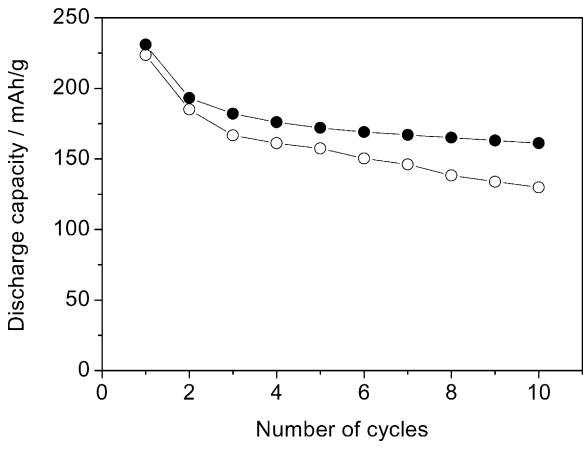

Fig. 4. Cycle performances of the (○) high-crystalline β-FeOOH electrodes, and (●) low-crystalline β-FeOOH electrodes.

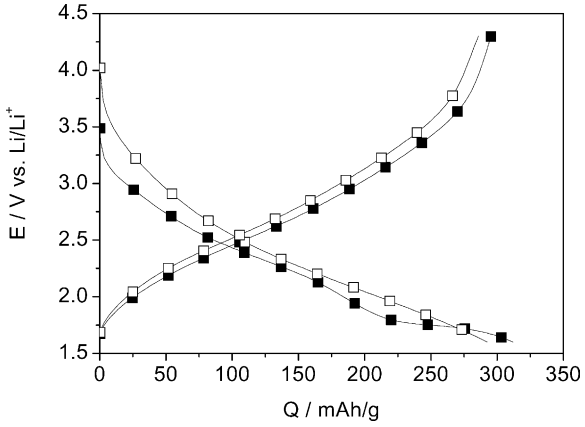

Fig. 5. Discharge and charge characteristics of the vanadium ferrite positive electrode in the (■) first and (□) second cycles.

The latter electrode exhibited better performance than the former. Two factors are proposed here to interpret this phenomenon; the crystalline structure and the particle morphology of the two samples. The effect of the crystallinity, however, seems to be relatively small, because a similar amorphous structure was formed during the first discharge for each electrode as mentioned above. Thus, the better cycle performance of the low-crystalline β-FeOOH electrode in the following cycles must result from the aggregated particle morphology of the active material rather than its lower crystallinity, because the aggregated particle is advantageous to maintain better electronic contact between primary particles.

3.3.2. *Vanadium ferrite positive electrode*

Fig. 5 represents the discharge and charge characteristics of the vanadium ferrite positive electrode in the first and second cycles. It gave an initial discharge capacity of 312 mAh/g. This remarkable high capacity can not be interpreted by the simple redox reaction of Fe^{2+}/Fe^{3+}, indicating that the reduction of vanadium contributed to the enhanced discharge capacity. Furthermore, a potential plateau appeared at around 1.8 V in the first discharge, and diminished in the second cycle, suggesting that the crystalline structure of the vanadium ferrite changed during the first cycle.

The structural change of the vanadium ferrite after the initial discharge and charge was investigated by XRD measurements. Fig. 6(a) and (b) show XRD patterns of the electrode discharged to 2.0 V and 1.6 V, respectively, and Fig. 6(c) presents that of the electrode charged to 4.3 V. The characteristic two peaks at around 28° and 30° of the active material (Fig. 1(c)) were still observed for the electrode discharged to 2.0 V (Fig. 6(a)). On the other hand, the intensity of these peaks drastically decreased at 1.6 V, and new peaks appeared at around 43° and 63° (Fig. 6(b)). These facts indicate that the electrochemical lithium intercalation into the vanadium ferrite occurred with less structural change at the potential range of 2.0 V and higher, while

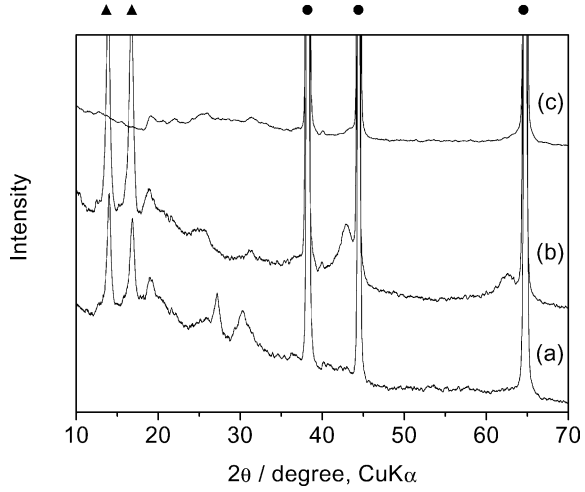

Fig. 6. XRD patterns of the vanadium ferrite positive electrode discharged to (a) 2.0 V and (b) 1.6 V, and charged to (c) 4.3 V in the first cycle. The discharged electrode was covered with liquid paraffin to inhibit the oxidation of the active material. Symbols (▲) and (●) denote the diffraction peaks due to liquid paraffin and aluminum, respectively. Small peaks at around 19 and 26° are due to PVdF and acetylene black, respectively.

its crystalline structure greatly changed during the potential plateau at around 1.8 V. The new peaks diminished for the electrode charged to 4.3 V (Fig. 6(c)), and a broad diffraction pattern was obtained. This result indicates that the vanadium ferrite became amorphous after cycling as in the case of β-FeOOH.

Comparing Fig. 2 with Fig. 5, the discharge potential of the vanadium ferrite electrode was found to be more positive than that of the β-FeOOH electrodes. The reduction of vanadium in the former electrode may contribute to the shift of its discharge potential in the positive direction.

Fig. 7 presents the cycle performance of the vanadium ferrite positive electrode. It maintained 82% of the initial discharge capacity at the 10th cycle, which is much higher than the value of 70% for the low-crystalline β-FeOOH electrode.

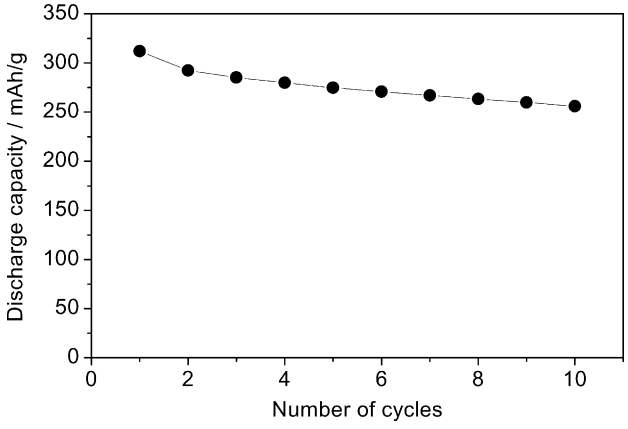

Fig. 7. Cycle performance of the vanadium ferrite positive electrode.

4. Conclusions

New iron-based oxides such as low-crystalline β-FeOOH and vanadium ferrite were prepared by a simple hydrolysis method. From the electrochemical measurements, it was found that the low-crystalline β-FeOOH positive electrode showed a discharge capacity of 230 mAh/g and better cycle performance than the high-crystalline one, and that the vanadium ferrite positive electrode also showed a high discharge capacity over 300 mAh/g and superior cycle performance. These oxides are considered to be promising candidates as the positive active materials of next-generation lithium secondary cells because of their easy synthesis method, high discharge capacity, and abundance.

References

[1] R. Kanno, T. Shirane, Y. Kawamoto, Y. Takeda, M. Takano, M. Ohashi, Y. Yamaguchi, J. Electrochem. Soc. 143 (1996) 2435.
[2] K. Ado, M. Tabuchi, H. Kobayashi, H. Kageyama, O. Nakamura, Y. Inaba, R. Kanno, M. Takagi, Y. Takeda, J. Electrochem. Soc. 144 (1997) L177.
[3] L. Bordet-Le Guenne, P. Deniard, A. Lecerf, P. Biensan, C. Siret, L. Fournes, R. Brec, Ionics 4 (1998) 220.
[4] A.K. Padhi, K.S. Nanjundaswamy, C. Masquelier, S. Okada, J.B. Goodenough, J. Electrochem. Soc. 144 (1997) 1609.
[5] A. Yamada, S.C. Chung, K. Hinokuma, J. Electrochem. Soc. 148 (2001) A224.
[6] H. Sakaebe, S. Higuchi, K. Kanamura, H. Fujimoto, Z. Takehara, J. Electrochem. Soc. 142 (1995) 360.
[7] N. Imanishi, T. Morikawa, J. Kondo, R. Yamane, Y. Takeda, O. Yamamoto, H. Sakaebe, M. Tabuchi, J. Power Sources 81–82 (1999) 530.
[8] K. Amine, H. Yasuda, M. Yamachi, J. Power Sources 81–82 (1999) 221.
[9] P. Poizot, E. Baudrin, S. Laruelle, L. Dupont, M. Touboul, J.-M. Tarascon, Solid State Ionics 138 (2000) 31.
[10] T. Ishikawa, K. Inoue, Bull. Chem. Soc. Jpn. 46 (1973) 2665.